ACS OMEGA

http://pubs.acs.org/journal/acsodf

Article

Microbial Carbonation of Monocalcium Silicate

Michael S. Guzman, Jaisree Iyer, Paul Kim, Daniel Kopp, Ziye Dong, Paniz Foroughi, Mimi C. Yung, Richard E. Riman,* and Yongqin Jiao*

Cite This: *ACS Omega* 2022, 7, 12524−12535

Read Online

ACCESS | Metrics & More | Article Recommendations | Supporting Information

ABSTRACT: Biocement formed through microbially induced calcium carbonate precipitation (MICP) is an emerging biotechnology focused on reducing the environmental impact of concrete production. In this system, CO_2 species are provided via ureolysis by *Sporosarcina pasteurii* (*S. pasteurii*) to carbonate monocalcium silicate for MICP. This is one of the first studies of its kind that uses a solid-state calcium source, while prior work has used highly soluble forms. Our study focuses on microbial physiological, chemical thermodynamic, and kinetic studies of MICP. Monocalcium silicate incongruently dissolves to form soluble calcium, which must be coupled with CO_2 release to form calcium carbonate. Chemical kinetic modeling shows that calcium solubility is the rate-limiting step, but the addition of organic acids significantly increases the solubility, enabling extensive carbonation to proceed up to 37 mol %. The microbial urease activity by *S. pasteurii* is active up to pH 11, 70 °C, and 1 mol L^{-1} $CaCl_2$, producing calcite as a means of solidification. Cell-free extracts are also effective albeit less robust at extreme pH, producing calcite with different physical properties. Together, these data help determine the chemical, biological, and thermodynamic parameters critical for scaling microbial carbonation of monocalcium silicate to high-density cement and concrete.

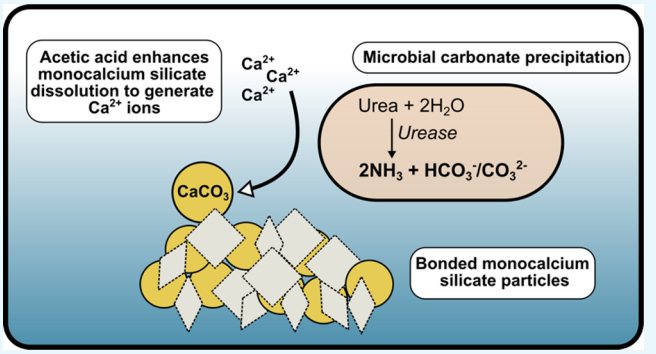

INTRODUCTION

Cement and concrete are the most widely used man-made materials and dramatically shape our built environment. Unfortunately, the cement industry is one of the largest industrial sources of pollution. Hydraulic Portland cement production accounts for 5−7% of global anthropogenic CO_2 emissions.[1] This is because the synthesis of Portland cement is energy-intensive, in part due to limestone calcination whereby limestone ($CaCO_3$) is thermally decomposed at high temperatures (∼1450 °C) into lime (CaO), and also because high-temperature solid-state diffusion is required to form the hydraulic di- and tricalcium silicates.[1,2] Recently, a low-energy carbonate cement concrete technology was invented by the Riman research group at the Rutgers University.[3−8] The technology consists of two innovative components. First, nonhydraulic cement based on monocalcium silicate is used because it can be synthesized at a temperature that is 250 °C lower than that for Portland cement and uses significantly less limestone, which reduces the energy and CO_2 emissions by 30%. Second, a process called low-temperature solidification (LTS) is used to carbonate the cement and aggregate mixture to form concrete.[3−8] LTS relies on infiltrating a particle network (monocalcium silicate and aggregate) with external CO_2, resulting in a coupled mineral dissolution−precipitation reaction product that fill concrete pore spaces as a means of solidification. This results in a densified, carbonate-bonded material with high compressive strength.

This technology has two technical barriers to overcome. First, it is not suitable for structures where the thinnest of three dimensions has greater than 30 cm of infiltration.[6] Second, the quantities of CO_2 required for typical projects (e.g., roads) are hundreds of tons of CO_2 per mile, much larger than the amounts of CO_2 available from the CO_2 industry within a typical delivery distance. Both problems will be solved if CO_2 is generated uniformly within the concrete structure. One approach for homogeneous, *in situ* CO_2 generation utilizes urea hydrolysis (ureolysis) by the bacterium *Sporosarcina pasteurii* (*S. pasteurii*) through a process called microbially induced calcium carbonate precipitation (MICP). However, past ureolysis-based studies utilize fully soluble calcium species (e.g., calcium chloride) for calcium carbonate precipitation.[9−11] In this case, all calcium species are immediately available, leaving the kinetics of the process solely dependent on the CO_2-based species. In contrast, carbonation of

Received: September 22, 2021
Accepted: March 24, 2022
Published: April 6, 2022

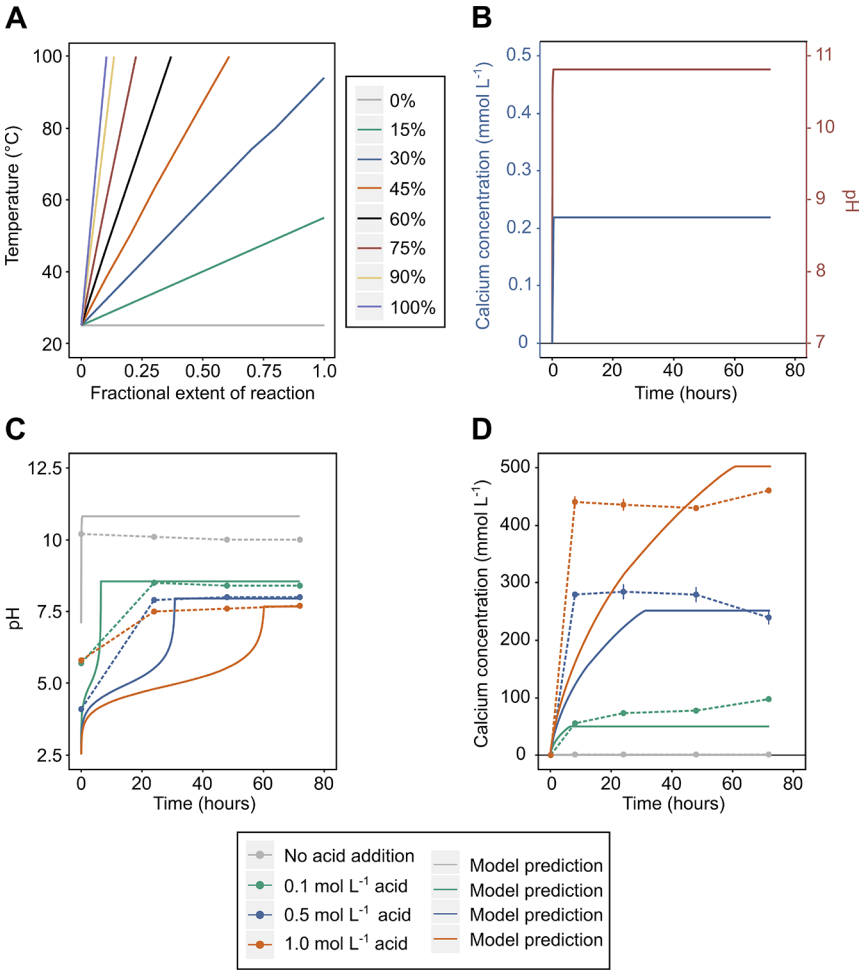

Figure 1. Modeling of ICD and calcium carbonation. (A) Model predictions for the increase in the temperature of slurries (i.e., a solid-to-liquid ratio of 0−100 wt %) under adiabatic conditions due to the exothermic heat of reaction associated with monocalcium silicate carbonation. (B) Model predictions for pH and calcium concentration evolution in a 15 wt % monocalcium silicate suspension. Experimental and modeled pH (C) and soluble calcium concentration (D) with the addition of acetic acid (0, 0.5, and 1 mol L^{-1}) to monocalcium silicate (15 wt %). Experimental data shown are the averages of replicates ± standard deviation (n = 3).

monocalcium silicate relies on a heterogeneous reaction involving incongruent calcium dissolution (ICD), a process where the acidic aqueous solution extracts calcium ions while the silica phase remains as a fugitive particle.[3−8] A major advantage of using a solid phase is it allows a higher volume of calcium delivered per unit volume as well as the use of particle size to control the release of calcium ions as a means to regulate the nucleation rate. Thus, kinetic processes involving the release of either soluble calcium by mineral dissolution or CO_2 species produced by microbial processes can be rate-limiting.

While a microbial process using monocalcium silicate offers many advantages, it has many more variables to control compared to fully soluble forms of calcium. Overall, the challenges of using biological mechanisms to carbonate monocalcium silicate include the low rate of ICD,[12−14] balancing the rate of microbial CO_2 production with ICD, and passivation of the mineral surface by precipitated calcium carbonates.[12] The first step in the development of such microbially driven carbonate cement concrete requires a fundamental understanding of how the kinetics of calcium carbonate formation is moderated by both ICD and microbially driven CO_2 species release. Past work has not reported any fundamental studies involving a solid phase as a calcium source, such as monocalcium silicate. Thus, this study focuses on the feasibility of microbial calcium carbonate crystallization involving a heterogeneous reaction of monocalcium silicate and microbially sourced CO_2. We chose to use a dilute suspension (i.e., slurry) to avoid additional complexities caused by high solid loadings commonly used in cement, mortar, and concrete systems. The high concentration of monocalcium silicate and aggregate (e.g., sand and gravel) creates a broad range of chemical and physical complexities, which will be covered in a future study. At a high concentration, monocalcium silicate cement primary particles can form agglomerates, which then pack densely and aggregate. These structural components physically change the reaction conditions by confining cells, reactants, and products to create chemical gradients in pH, dissolved calcium and CO_2 species, and calcium carbonate that would not be observed in a dilute slurry. Thus, the purpose of this current study is to observe how microbial species carbonate the calcium emanating from a dilute concentration of monocalcium silicate and to identify the complexities, which will be relevant to concrete-forming systems.

https://doi.org/10.1021/acsomega.1c05264
ACS Omega 2022, 7, 12524−12535

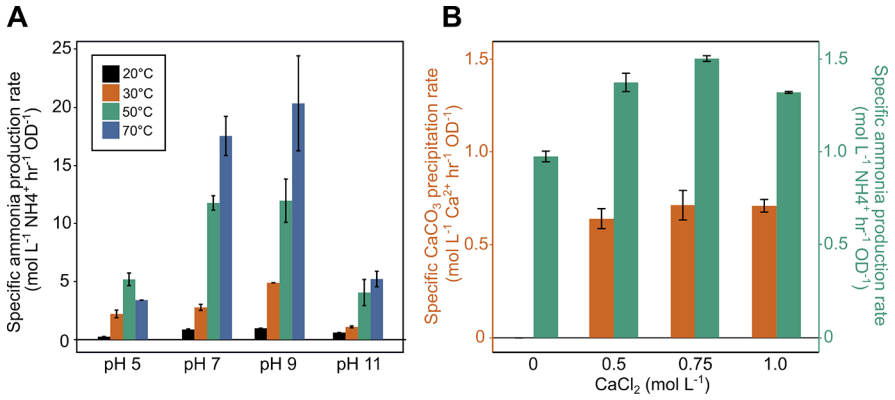

Figure 2. Effect of temperature, pH, and calcium salt concentration on urease activity of *Sporosarcina pasteurii* ATCC 11859. (A) Effect of temperature and pH on urease activity. (B) Influence of calcium salt ($CaCl_2$) concentration on urease activity and the calcium carbonate ($CaCO_3$) precipitation rate. Data shown are the averages of biological replicates assayed in triplicate ± standard deviation (n = 3).

Here, we present a microbial cement curing concept whereby ureolysis by *S. pasteurii* releases CO_2 *in situ* to catalyze MICP from calcium ions released from mineral-based monocalcium silicate, where internally produced microbially generated CO_2 circumvents the diffusion limitations of externally supplied CO_2. We characterized the microbiological and geochemical processes involved and developed thermodynamic and chemical kinetic models trained on experimental data.

RESULTS AND DISCUSSION

Kinetic and Thermodynamic Modeling of ICD and Calcium Carbonation. Thermodynamic and chemical kinetic models were developed to identify the geochemical conditions that microbes are subjected to during ICD and carbonation and to predict rate-limiting geochemical processes. We focused on modeling a dilute slurry (15 wt %) where experimental parameters are easily probed and hence provide a basic understanding of the reaction and crystal growth kinetics and mechanisms associated with both the cells and inorganic chemistry. This insight enables us to anticipate problems and propose design solutions to overcome these limitations. An adiabatic thermal model was developed to predict the temperature as a function of reaction conditions and the carbonation reaction extent (Figure 1A). This model demonstrates the final temperature increases with the fractional carbonation reaction extent under all solid loading conditions tested (i.e., a solid-to-liquid ratio of 0−100 wt %). The results shown in Figure 1A are upper limits that do not account for the heat loss to the environment. For a low solid fraction of 15 wt % and complete carbonation of monocalcium silicate, the temperature reaches a maximum of 55 °C (Figure 1A, green line), which is acceptable for our microbial urease. However, urease activity can only withstand a temperature not greater than 70 °C under extended reaction periods. Thus, unless there is a suitable mechanism for the heat loss, solid loadings significantly greater than 15 wt % have the capability to exceed this temperature and negatively impact the microbial activities.

The chemical kinetic model was used to predict the solution conditions of the heterogeneous monocalcium silicate slurry system. In the absence of CO_2, a slurry of monocalcium silicate at 15 wt % results in an equilibrium solution pH of 10.8 and a soluble calcium concentration of 0.22 mmol L^{-1} (Figure 1B). This high pH poses a challenge for microbial carbonation by significantly lowering the rate of ICD, thus slowing down the carbonation process. The rate of ICD can be increased considerably by lowering the solution pH (eq 13). For example, the rate of ICD at pH 5 (4.90×10^{-13} mol cm^{-2} s^{-1}) is nearly an order of magnitude higher than that at pH 10 (6.17×10^{-14} mol cm^{-2} s^{-1}). In addition, the high pH hinders the microbial ureolysis rate, which is optimal at pH 9 and is 80% lower at pH 10.[15] Thus, a lower pH caused by the introduction of acidic species could improve both ICD and CO_2 release rates, both of which contribute to an increased extent of reaction.

Addition of Organic Acids Enhances Incongruent Calcium Dissolution. Based on the results from chemical kinetic modeling, we hypothesized that supplementing cement slurries with acid will accelerate ICD rates and thus provide a high reservoir of soluble calcium for MICP[11] as well as enhance microbial ureolysis rates.[9,15−17] This approach has been applied in biocementation studies to enhance the dissolution of carbonate rocks and has demonstrated strength improvements in sand columns correlated with microbial $CaCO_3$ precipitation from $CaCl_2$ solutions.[11,18,19] We aimed to adopt these approaches in our process wherein ureolytic microbes, when incubated in acid-treated monocalcium silicate slurries, increase the extent of $CaCO_3$ precipitation that bonds unreacted and partially reacted monocalcium silicate particles, as well as aggregate phases.

Among the different types of inorganic and organic acids, we chose organic acids because they are biocompatible and microbially produced at the industrial scale sustainably.[20] We examined the effect of acetic acid addition on ICD at varying acid concentrations and pH values in a 15 wt % cement slurry system. Thermodynamic modeling predicted equilibrium pH values of 8.5, 7.9, and 7.6 for acetic acid systems at concentrations of 0.1, 0.5, and 1 mol L^{-1}, respectively (Figure 1C). Chemical kinetic modeling predicted that the addition of acetic acid enhances ICD rates (Figure 1D). However, the model predicted slower dynamics than experimental observations (Figure 1C,D). For example, the experimental data reach the equilibrium pH earlier than model predictions, which tracks the measured soluble calcium levels (Figure 1C,D). This discrepancy could be due to uncertainty in model parameters such as the monocalcium silicate surface area[13] and the rate expression in eq 13. Overall, these results confirm that lowering the pH increases the ICD rate, which enables higher microbial carbonation rates and extent of reaction.

https://doi.org/10.1021/acsomega.1c05264
ACS Omega 2022, 7, 12524−12535

Urease Activity Is Robust under Cement Curing Conditions. Cement curing could pose a unique challenge for MICP due to the extreme conditions that microbes/enzymes are exposed to, including alkaline pH and elevated temperatures (Figure 1). Previous studies have examined urease activity under various pH and temperature regimes.[16] However, a comprehensive understanding of how both urease activity and $CaCO_3$ precipitation rates change as functions of the reaction temperature, pH, and ionic strength has been lacking. To gain a better understanding of the boundary conditions for microbial urease activity, we examined the effect of pH (5−11), temperature (20−90 °C), and soluble calcium concentration (0−1 mol L^{-1} $CaCl_2$) on whole-cell urease activity and the calcium carbonate biomineralization rate by *S. pasteurii*. We chose *S. pasteurii* for our studies due to its high ureolytic activity relative to other urease-positive bacterial strains based on a microbial screen that we performed (Figure S1).

We observed that the *S. pasteurii* urease activity is strongly pH- and temperature-dependent (Figure 2A) with an optimum pH range of 7−9 and a temperature range of 50−70 °C. A sharp decrease in urease activity is observed at both pH 5 and 11 and temperatures of 20 and 30 °C. The temperature-dependent increase in ureolysis cannot be explained by the rate of thermal urea degradation because the rate of this reaction is far smaller than that of the observed urease activity (Table S1). Overall, these results show that urease activity is maintained throughout the ICD process. Lowering the pH to between 7 and 9 further enhances the urease activity, especially at temperatures above 30 °C.

Finally, our chemical kinetic modeling shows that acetic acid enhances ICD by increasing the amount of soluble calcium (Figure 1D). There is a possibility that the high amount of calcium ions produced from ICD could diminish whole-cell urease activity, which in turn inhibits carbonation. Additionally, high calcium concentrations leading to abundant $CaCO_3$ precipitation by ureolytic bacteria can also result in cell encasement,[21] which also limits microbial activity. Whether this results in subsequent microbial inactivation, however, is unclear.[22,23] Here, we examined the effect of calcium ion concentration on urease activity and the calcium carbonate biomineralization rate. The urease activity remained the same up to 1 mol L^{-1} $CaCl_2$ with a peak occurring at 0.75 mol L^{-1} $CaCl_2$ (~1.5 mol L^{-1} Ca^{2+} h^{-1} OD^{-1}) (Figure 2B). Calcium biomineralization tracks urease activity and is ~1/2 the rate of urease activity at each tested $CaCl_2$ concentration (e.g., ~0.75 mol L^{-1} Ca^{2+} h^{-1} OD^{-1} at 1 mol L^{-1} $CaCl_2$) (Figure 2B). A similar effect on *S. pasteurii* urease activity was observed with the addition of calcium nitrate in a previous study.[17] Overall, these studies indicate that the *S. pasteurii* urease activity can be maintained during cement carbonation where soluble calcium concentration is up to 1 mol L^{-1}.

Whole-Cell-Catalyzed Carbonation Is Enhanced by Acetic Acid Addition. Given that acetic acid enhanced the rate of ICD (Figure 1D), we hypothesized that the addition of an acid will increase the microbial $CaCO_3$ precipitation. To determine if acid pretreatment improves the extent of $CaCO_3$ precipitation, we assayed the microbial activity in dilute slurries (15 wt %) treated with a range of acetic acid concentrations (0−1 mol L^{-1}). We chose a dilute slurry system for this study to assess the microbial activity rates and compare them to model predictions.

To model the carbonation behavior of the monocalcium silicate−acetic acid system, kinetic simulations for microbial ureolysis were performed on a system that had achieved equilibrium (i.e., end points in Figure 1C,D). The ureolysis kinetic model predicted that the ammonia production rate stays the same irrespective of the concentration of the added acetic acid (Figure 3A). The experimentally determined

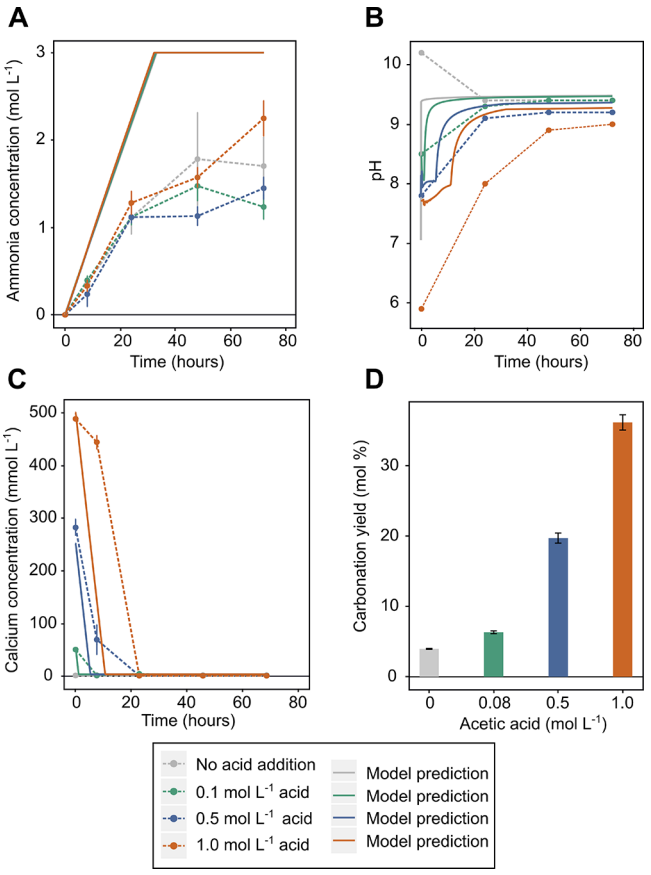

Figure 3. Whole-cell-induced carbonation of acetic acid-treated monocalcium silicate slurries. Experimental and modeled (A) ammonia production, (B) pH, (C) soluble calcium concentration, and (D) calcium carbonate precipitation with the addition of acetic acid (0, 0.5, and 1 mol L^{-1}) to 15 wt % (i.e., the solid-to-liquid ratio) monocalcium silicate slurries. Data shown are the averages of biological replicates assayed in triplicate ± standard deviation (n = 3).

ammonia production rates for *S. pasteurii* were similar across the acid concentrations in the first 24 h of incubation (~0.05 mol L^{-1} NH_4^+ h^{-1}) but were lower than model predictions (Figure 3A). This discrepancy could be attributed to a variety of factors, including a decrease in microbial urease activity due to the nonoptimal initial pH of the system (Figure 1C), decreasing substrate concentration, or high ammonium ion concentrations.[17] The production of ammonia was accompanied with an increase in pH, which approached pH 9−9.5 after 40 h toward the equilibrium (Figure 3B). The model predictions for pH evolution showed a similar trend to the experimental observations (Figure 3B).

The model was also used to predict the rate of $CaCO_3$ precipitation from the experimentally determined rate of urease activity (Figure S2). Incubation of monocalcium silicate with acetic acid (prior to introduction of microbial ureolysis in the model) results in the buildup of calcium ion concentration

https://doi.org/10.1021/acsomega.1c05264
ACS Omega 2022, 7, 12524−12535

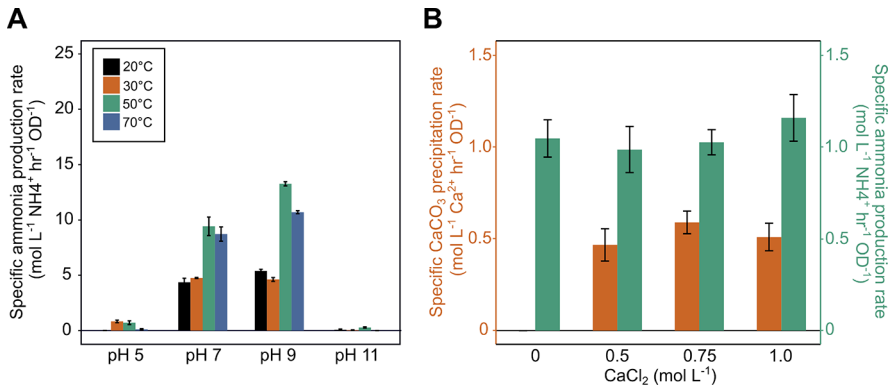

Figure 4. Effect of temperature, pH, and calcium salt concentration on cell-free extract urease activity. (a) Effect of temperature and pH on urease activity of cell-free extracts. (b) Influence of calcium salt ($CaCl_2$) concentration on urease activity and the calcium uptake rate of cell-free extracts. Data shown are the averages of biological replicates assayed in triplicate ± standard deviation (n = 3).

as noted by the higher initial calcium concentration (Figure 3C). Due to the availability of soluble calcium, the initial carbonation rate upon introduction of ureolysis is rapid and is limited by the production of CO_2 (46 mmol L^{-1} h^{-1}) (Figure S2). Conversely, once the soluble calcium is converted to $CaCO_3$, the carbonation rate drops to 0.9 mM/h as the rate of ICD again becomes limited. The model predicts a higher initial carbonation rate than experimental observations (Figure 3C). This is primarily due to the model overprediction of the rate of urease activity (Figure 3A) as it does not account for the various factors mentioned above that could compromise microbial activity.

The $CaCO_3$ content in the solids was determined by calcimetry to confirm biomineralization. This analysis demonstrated that the carbonate yield stoichiometrically increased with acetic acid concentration up to 1 mol L^{-1}, equivalent to a theoretical yield of 37 mol % conversion of $CaSiO_3$ to $CaCO_3$ after 72 h of incubation (Figure 3D; eqs 19 and 20). The extent of monocalcium silicate carbonation strongly correlates with the soluble calcium content, demonstrating that organic acid leaching is an effective means of increasing microbial carbonation.

The Cell-Free Extract Is an Effective Catalyst for Monocalcium Silicate Carbonation. Traditionally, in biocement, whole cells are used for carbonation.[24] In the case of ureolysis, a single enzyme (urease) hydrolyzes urea to form ammonia and CO_2, which elevates the solution pH and catalyzes $CaCO_3$ precipitation.[24] In this whole-cell scheme, the bacterial membrane provides a stable microenvironment for cellular activities, such as buffering intracellular pH and the ion content. However, utilizing whole cells for cement carbonation requires that bulky (micrometer scale) cellular biomass is distributed within a pore size large enough to accommodate the microbes and the distribution of these pores is uniform,[25] which could limit the types of possible concrete microstructures. To avoid this concern, we tested a cell-free approach, where *S. pasteurii* cell-free extracts containing the urease enzyme are used as the catalyst to decompose urea for $CaCO_3$ precipitation. This approach eliminates the need for cells, enables more even distribution of the reactants in cement, and accommodates a wider range of cement and concrete microstructures, all of which could result in better mechanical properties.[26] The feasibility of this approach has been demonstrated in previous studies where cell-free extracts were utilized for soil stabilization,[27] sand consolidation,[26] and concrete crack repair.[28]

Our data show that cell-free extracts have effective urease activity over a wide range of conditions, but the activity appears not as robust as that of whole cells (Figure 4). In contrast to whole cells that exhibited the maximum activity at 70 °C, the maximum activity for cell-free extracts was observed at 50 °C, indicating lower heat stability of cell-free extracts than that of whole cells (Figure 4A). Similar to whole cells, the optimum pH for cell-free extracts was 7−9 (Figure 4A). However, the activity in cell-free extracts is more significantly hindered at pH 5 and pH 11 (5% and 2% of the maximum activity, respectively, relative to that at pH 9, 50 °C) than the whole-cell activity (44% and 34% of the activity, respectively, relative to that at pH 9, 50 °C). Finally, cell-free extracts maintain a high soluble calcium salt tolerance, similar to whole cells, and the $CaCO_3$ precipitation rates remained the same upon addition of up to 1 mol L^{-1} $CaCl_2$ (Figure 4B). Our results indicate a potential limitation to using cell-free extracts: without the protective cell membrane, the urease enzyme is more sensitive to environmental conditions with lower carbonation rates.

To determine if the cell-free extract is active and capable of catalyzing $CaCO_3$ precipitation, we incubated cell-free extracts in acetic acid-treated monocalcium silicate (15 wt %) and monitored the urease enzyme activity, pH, and the calcium biomineralization rate (Figure 5). We observed high-level urease activity in monocalcium silicate slurries demonstrated by ammonia production and the calcium biomineralization rate (Figure 5A−C). Calcimetry performed on these samples indicated that $CaCO_3$ precipitation by cell-free extracts is similar to whole cells at the end of 72 h of incubation (Figure 5D). These data suggest that the urease enzyme in cell-free extracts is active and can catalyze $CaCO_3$ precipitation. However, its activity is more susceptible to environmental conditions, especially at pH values below 7 and above 9 (Figure 4), which could influence its stability during prolonged incubation under cement conditions.

Whole Cells and Cell-Free Extracts Both Produce Calcite Minerals but with Different Morphologies. The availability of nucleation sites is an important factor that regulates $CaCO_3$ biomineralization. It has been suggested that the bacterial cell surface, along with organic macromolecules, plays a role in $CaCO_3$ crystal nucleation.[29,30] However, other factors such as the presence of inorganic particles (e.g.,

https://doi.org/10.1021/acsomega.1c05264
ACS Omega 2022, 7, 12524−12535

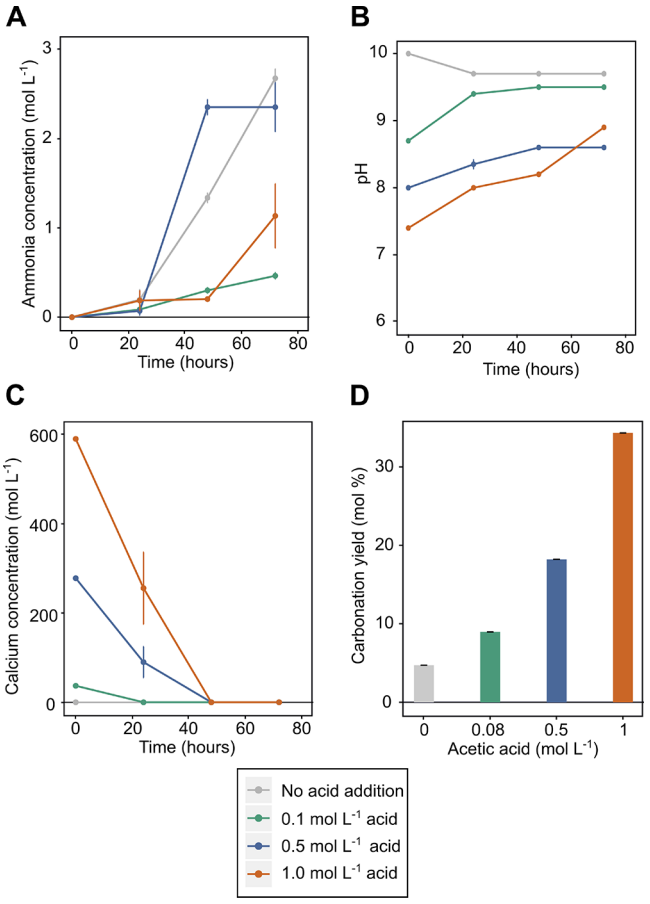

Figure 5. Cell-free extract-induced carbonation of acetic acid-treated monocalcium silicate slurries. Experimentally determined (A) ammonia production, (B) pH, (C) soluble calcium concentration, and (D) calcium carbonate precipitation with the addition of acetic acid (0, 0.5, and 1 mol L^{-1}) to 15 wt % (i.e., the solid-to-liquid ratio) monocalcium silicate slurries containing cell-free extracts. Data shown are the averages of biological replicates assayed in triplicate ± standard deviation (n = 3).

monocalcium silicate) and organic constituents (e.g., acetic acid, acetate ions, and hydronium ions) could also influence the physical properties of precipitated $CaCO_3$. To characterize the mineral phase and morphology of the $CaCO_3$ formed, we performed scanning electron microscopy (SEM), elemental mapping, and powder X-ray diffraction (XRD) of incubated monocalcium silicate slurries amended with acetic acid. This analysis revealed the presence of $CaCO_3$ crystals in slurries amended with both whole cells (Figure 6A) and cell-free extracts (Figure 6B). EDS analysis of the crystalline regions showed primarily calcium, carbon, and oxygen peaks indicative of $CaCO_3$ (table insets in Figure 6C,D). Powder X-ray diffraction (XRD) confirmed the presence of primarily calcite in both cases and correlated the increasing concentration of calcite with the increasing concentration of acetic acid (Figure 7). In addition, the calcite crystals covered the surface of monocalcium silicate particles, serving to connect the particles together. A distinct difference in the minerology morphology was observed between whole cells and cell-free extracts (Figure 6C,D). Whole-cell incubations yielded calcite of smaller and more irregular shape, whereas cell-free extracts led to the precipitation of larger and more cuboidal-shaped crystals. These data demonstrate that *S. pasteurii* urease can facilitate calcite formation from monocalcium silicate and that the choice of biocatalyst (whole cells versus cell-free extracts) plays an important role in the morphology of $CaCO_3$ precipitation.

This study has provided us with numerous guidelines instructive to the formulation of cements, mortar, and concrete. First, the solid content of any type of cement product will always exceed 15 wt %. Thus, the heat output from the overall process must be controlled to be not warmer than 70 °C. Second, the high solid loading will also increase the system pH. While this issue can be managed by the addition of acetic acid, the cement particles will neutralize a good portion of the acid added. Thus, time must be taken for the acid addition so that the solution pH does not drop below 5 but not too slow that the pH goes above 9. Another precaution associated with acid addition is to avoid the accumulation of too much soluble calcium, as a concentration of 3 mol L^{-1} soluble calcium or higher will inhibit urease activity. Finally, the use of a cell lysate solution containing the urease enzyme alleviates the concern regarding accommodation of the microbes in the cement or cement−aggregate microstructure. However, this advantage has a trade-off given the fact that a temperature of 50 °C yields a higher activity than that of 70 °C, and the calcium carbonate output with the lysate is far less than that with the intact microbes, which is likely caused by the diminished activity and stability of the urease enzyme in the lysate during reaction progression. Overall, these experiments provide an informative preview of this system as being highly sensitive to many processing variables. We can expect to see both differences and similarities as these experiments are modified for making cement or concrete.

CONCLUSIONS

Our work demonstrates the initial feasibility of using MICP to catalyze $CaCO_3$ precipitation from monocalcium silicate. While our experiments were carried out in far more dilute conditions, using particle dispersions instead of particle compacts, the complexity of MICP has been revealed. This study shows every variable, whether solids loading, pH, dissolved calcium, organic acid concentration, or the use or absence of cells, is important and must be optimized to ensure the cells catalyze carbonation of calcium silicate. These experiments along with the process modeling give an informative preview of the complexities to expect when formulating mortar or concrete.

METHODS

Bacterial Strains and Culture Conditions. *Sporosarcina pasteurii* ATCC 11859, *Lysinibacillus sphaericus* (*L. sphaericus*) ATCC 14577, *Bacillus megaterium* (*B. megaterium*) ATCC 14581, and *Bacillus saliphilus* (*B. saliphilus*) BAA-957 were acquired from the ATCC (American Type Culture Collection). Lyophilized cells were propagated in sterile liquid growth media (autoclaved at 121 °C for 30 min) and cultivated according to the ATCC recommendations for each strain. The cultivation conditions used for each strain were as follows: *S. pasteurii* ATCC 11859 (Tris-yeast extract; 0.13 mol L^{-1} Tris, pH 9.0, 20 g L^{-1} yeast extract, 10 g L^{-1} ammonium sulfate; 30 °C); *L. sphaericus* ATCC 14577 (beef extract adjusted to pH 7.2; 10 g L^{-1} beef extract, 10 g L^{-1} yeast peptone, 10 g L^{-1} NaCl; 30 °C); *B. saliphilus* BAA-957 (tryptic soy broth-NaCl adjusted to pH 9.0; 30 g L^{-1} CASO, 160 g L^{-1}

https://doi.org/10.1021/acsomega.1c05264
ACS Omega 2022, 7, 12524−12535

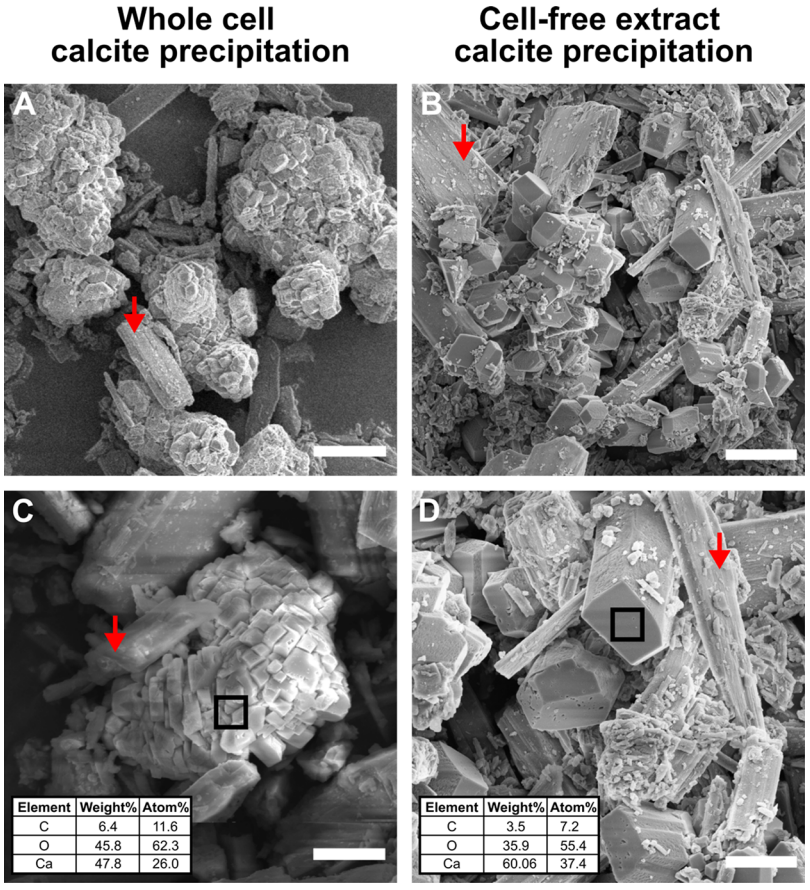

Figure 6. SEM and EDS analysis of whole-cell- and cell-free extract-induced calcium carbonate precipitation. SEM images of 15 wt % monocalcium silicate slurries (i.e., the solid-to-liquid ratio) pretreated with 1 mol L^{-1} acetic acid and amended with either whole cells (A,C) or cell-free extracts (B,D). Scale bars: 10 (A,B) and 5 μm (C,D). Elemental analysis of crystal regions is indicated by the black box (all elements detected are shown in table insets in (C) and (D)). Red arrows indicate representative monocalcium silicate particles.

NaCl; 37 °C); and *B. megaterium* ATCC 14581 (8 g L^{-1} BD 234000 Difco Nutrient broth; 30 °C). For all experiments, cells were cultivated in shaking incubators held at 150 rpm until they reached the mid-exponential phase of growth. The biomass concentration was determined by measuring the optical density (at 600 nm) using a 96-well plate reader (BioTek, USA). An optical density (OD) of 1.0 was defined as 1×10^9 cells mL^{-1} based on the conversation factor used by Lauchnor *et al.*[15]

Ammonia Determination. Ammonia concentrations were determined using the Berthelot reaction procedure using a standard curve of known concentrations of ammonium chloride (0−500 μmol L^{-1}).[31] Briefly, samples and standards were diluted in deionized water (Milli-Q water, 18.2 mΩ), and 100 μL of the sample was mixed with 75 μL of a color reagent (27 mg mL^{-1} sodium salicylate and 1 mg mL^{-1} sodium nitroprusside dehydrate in 0.5 mol L^{-1} NaOH) and 25 μL of oxidation solution (3% sodium hypochlorite in 1 mol L^{-1} NaOH) in a 96-well plate. All reagents were stored at 4 °C and brought to room temperature before use. Samples were incubated on an orbital plate shaker (800 rpm) for 5 min at 30 °C, and absorbance was measured (670 nm).

Ureolysis Rates. Pregrown bacterial cultures were centrifuged at 5000*g* for 10 min and washed with sterile 0.85% NaCl. Cultures were then resuspended in buffered ureolysis media, which consisted of 0.66 mol L^{-1} urea dissolved in buffer. Standard ureolysis rate experiments for all strains were carried out in urea-sodium phosphate (0.1 mol L^{-1}, pH 7) solutions held stationary at 30 °C in sealed containers. Temperature versus pH experiments were conducted in the following buffers at a concentration of 0.1 mol L^{-1}: sodium citrate (pH 5), sodium phosphate (pH 7), bicine (pH 9), and sodium carbonate (pH 11). The starting optical density used in ureolysis rate experiments was 0.025 unless otherwise noted. When *S. pasteurii* cell-free extracts were used, the urease activity was normalized to whole-cell activity. Urease activity rates were determined by measuring the ammonia concentration (via the Berthelot method) every 12 min for 1 h.

Calcium Carbonate Precipitation Rates. For calcium biomineralization rate experiments, $CaCl_2$ was dissolved in urea-sodium phosphate (pH 7). For calcium salt inhibition experiments where up to 1 mol L^{-1} $CaCl_2$ was used, $CaCO_3$ precipitation and ammonia production rates were determined by sampling over a 24 h period. The starting optical density used in experiments was 0.1, and all experiments were carried out at 30 °C in sealed containers.

Calcium Determination. Soluble calcium was determined using a colorimetric calcium assay (assay reagent = ethanolamine (0.375 mol L^{-1}, pH 10.6), *o*-cresolphthalein complexone (82.0 μmol L^{-1}), 8-hydroxyquinoline (7.16 mmol L^{-1}), and hydrochloric acid (27.75 mmol L^{-1})) with comparison to a standard curve of known concentrations of $CaCl_2$ (0−5 mmol L^{-1}). Samples and standards were diluted in deionized

https://doi.org/10.1021/acsomega.1c05264
ACS Omega 2022, 7, 12524−12535

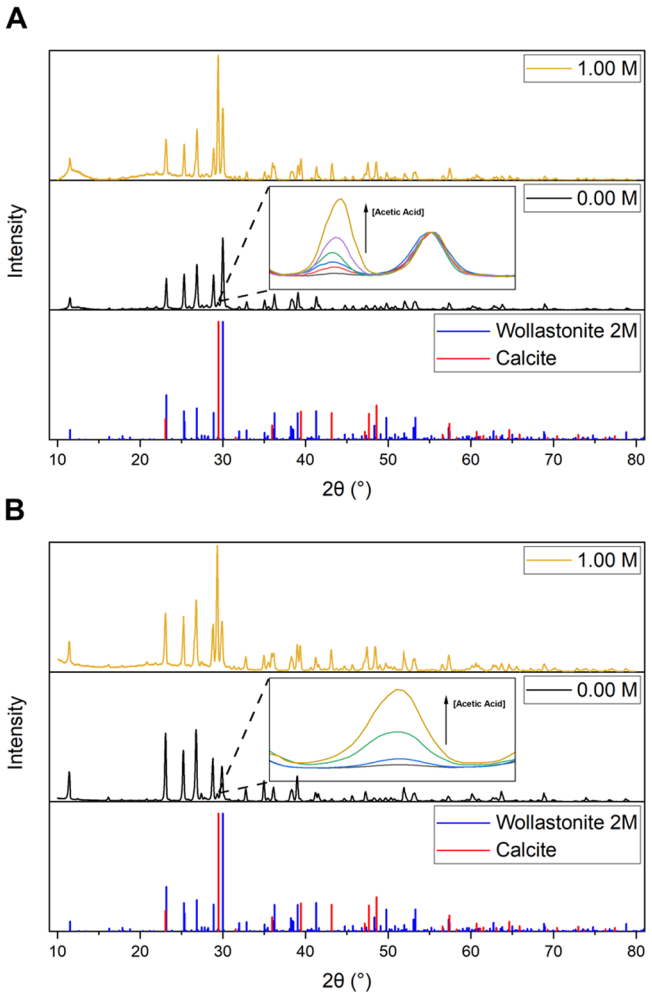

Figure 7. XRD analysis of whole-cell- and cell-free extract-induced calcium carbonate precipitation. X-ray diffraction of 15 wt % (i.e., the solid-to-liquid ratio) monocalcium silicate slurries amended with either whole cells (A) or cell-free extracts (B). The top (yellow) spectrum of each graph shows monocalcium silicate slurries treated with 1 mol L^{-1} acetic acid and either whole cells (A) or cell-free extracts (B). The middle (black) panel shows spectra for abiotic, untreated monocalcium silicate slurries (negative control). The inset spectra in the middle panels indicate monocalcium silicate slurries treated with increasing concentrations of acetic acid (0−1 mol L^{-1}) and either whole cells (A) and cell-free extracts (B). The calcite peak is shown to increase with increasing acetic acid concentration. Reference spectra for monocalcium silicate (Wollastonite 2M, blue) and calcite (red) are shown in the lower panel of each diagram.

water, and 5 μL was mixed with 95 μL of the assay reagent in a 96-well plate. All reagents were stored at 4 °C for no longer than 1 week and brought to room temperature before use. Samples were incubated on an orbital plate shaker (800 rpm) for 5 min at 30 °C, and absorbance was measured (570 nm). Rate measurements were normalized to the initial optical density.

Cement Bioslurry Composition. Cement slurries were prepared by suspending 15 wt % NYAD M400 monocalcium silicate (NYCO Minerals, Inc., USA) in deionized water. Before bacterial inoculation, slurries were incubated for at least 72 h abiotically at room temperature on a rotating shaker in sealed containers. Cells were washed at least once and resuspended in 0.85% NaCl. The starting optical density used in experiments was 0.1 unless otherwise noted. The pH was determined using a pH probe. Monocalcium silicate slurries (15 wt %) were increased in scale to ∼150 g to enable carbonate content analysis via calcimetry and XRD. These bioslurries were directly dosed with the requisite amount of glacial acetic acid (Fisher Scientific, Pittsburgh, Pennsylvania, USA) to achieve the desired acetic acid concentration (i.e., 0−1.0 mol L^{-1}). Slurries were also dosed with the requisite amount of Certified ACS urea (Fisher Scientific, Pittsburgh, Pennsylvania, USA) to achieve a concentration of 1.5 mol L^{-1}. After bacterial inoculation, the samples were incubated for 72 h on an orbital shaker in sealed containers before being harvested.

Cell Lysis. *S. pasteurii* cells (20 mL) were cultivated under standard conditions and centrifuged at 5000*g* at 4 °C for 15 min and resuspended in 4 mL of chilled 0.1 mol L^{-1} bicine buffer (pH 9). Phenylmethylsulfonyl fluoride (PMSF) (1 mmol L^{-1}) was added to resuspended cells before cell lysis. Bacterial cells were lysed using a French press at 14,000 psi. Cellular debris was removed by centrifuging samples at 10,000*g* for 20 min. Aliquots of the supernatant were stored in 5% glycerol at −80 °C until use.

Geochemical Modeling of Microbial Carbonation of Monocalcium Silicate. To understand the impact of the different microbial and chemical processes on the microbial carbonation of calcium silicate, we developed a simple numerical model. The model incorporates experimentally observed pH-dependent microbial ureolysis kinetics along with both kinetic and equilibrium reactions associated with the carbon, nitrogen, and calcium-based species. The key reactions included in the model are listed below:

$$NH_3 + H_2O \rightleftarrows NH_4^+ + OH^- \quad (1)$$

$$H_2CO_3 \rightleftarrows H^+ + HCO_3^- \quad (2)$$

$$HCO_3^- \rightleftarrows CO_3^{2-} + H^+ \quad (3)$$

$$H_2O \rightleftarrows H^+ + OH^- \quad (4)$$

$$CaSiO_3(s) + 2H^+ \rightleftarrows Ca^{2+} + SiO_2 + H_2O \quad (5)$$

$$CaCO_3(s) \rightleftarrows Ca^{2+} + CO_3^{2-} \quad (6)$$

Unless indicated by the subscript (s) to denote solid, all the species listed in the equations above are in an aqueous phase. Thus, eight aqueous species concentrations (excluding water as its concentration is assumed to remain unchanged) need to be computed to determine the state of the system. Typically, chemical reactions with solid minerals are slower than reactions between aqueous species.[32] Thus, eqs 1−4 are always assumed to be at equilibrium. The B-dot activity coefficient model was used to compute the activities of the aqueous species[33] as it is applicable for solutions with an ionic strength of about 1−2 M. The expression of the activity coefficient is shown below:

$$\log_{10}\gamma_i = \frac{-Az_i^2\sqrt{I}}{1 + a_iB\sqrt{I}} + \dot{B}I \quad (7)$$

where γ_i is the activity coefficient of species i; z_i is the charge of species i; A, B, and $\dot{B}$ are model-specific parameters; and a_i is the hard core diameter of species i. The values of the different parameters were obtained from the database in LLNL's EQ3/6 geochemical modeling software.[34] The activities of the solid phases and water were assumed to be 1.[32] This allows us to

https://doi.org/10.1021/acsomega.1c05264
ACS Omega 2022, 7, 12524−12535

relate the equilibrium constants for the six reactions listed above in terms of the concentrations of the aqueous species. For example, the equilibrium relation associated with eq 1 yields the following:

$$K_1 = \frac{\gamma_{NH_4^+}[NH_4^+]\gamma_{OH^-}[OH^-]}{\gamma_{NH_3}[NH_3]} \quad (8)$$

To solve for the state of the system, we need eight equations to determine the concentrations of the eight species. Four equations are obtained from the equilibrium constraints for reactions in eqs 1−4. The values of these equilibrium constants at 20 °C are listed in Table S2.[34] Three other equations are obtained by performing a mass balance on nitrogen, calcium, and carbon. They are as follows:

$$[NH_3]_t + [NH_4^+]_t = N_{tot,t} = N_{tot,t-1} + \Delta t \times r_{urease} \quad (9)$$

$$[Ca^{2+}]_t = Ca_{tot,t} = Ca_{tot,t-1} + \Delta t \times r_{wollastonite} - \Delta t \times r_{calcite} \quad (10)$$

$$[CO_3^{2-}]_t + [HCO_3^-]_t + [H_2C]_t = C_{tot,t} = C_{tot,t-1} + \frac{(N_{tot,t} - N_{tot,t-1})}{2} - \Delta t \times r_{calcite} \quad (11)$$

where N_{tot}, Ca_{tot}, and C_{tot} are the total amounts of nitrogen, calcium, and carbon in the system; the subscripts t and $t-1$ denote the current and previous time; Δt is the length of the time step; r_{urease} is the rate of urease activity, $r_{wollastonite}$ is the rate of monocalcium silicate dissolution (ICD), and $r_{calcite}$ is the rate of calcite precipitation, all in units of M/h. The final equation is a charge balance to ensure the electroneutrality of the solution. This yields the following:

$$2[Ca^{2+}] + [H^+] + [NH_4^+] - [OH^-] - [HCO_3^-] - 2[CO_3^{2-}] = 0 \quad (12)$$

To solve the system of equations, we need the initial nitrogen, calcium, and carbon concentrations, which are all 0, and expressions for r_{urease}, $r_{calcite}$, and $r_{wollastonite}$. r_{urease} is calculated by interpolating between experimentally determined values. In the absence of pH-dependent microbial calcite precipitation rates, we assumed that $r_{calcite} = \frac{r_{urease}}{2}$. This assumption would be reasonable if the rate of microbial calcite precipitation is significantly faster than the rate of microbial generation of CO_2 by ureolysis and is supported by the observations in Figure 2B. If the rate of generation of calcium ions is slower that the rate of CO_2 generation, then calcite will precipitate at an even slower rate due to the unavailability of calcium ions. By incorporating $r_{calcite}$ and $r_{wollastonite}$, the model can capture both types of rate limitations: CO_2 availability and Ca^{2+} availability (as shown in Figure S2).

Finally, $r_{wollastonite}$ was obtained from the data reported by Schott *et al.*[35]

$$r_{wollastonite} = a_v \left[\frac{cm^2}{L}\right] \times \begin{cases} 10^{-10}(\gamma_{H^+}[H^+])^{0.46}\left[\frac{mol}{cm^2 \cdot s}\right], & pH < 4.8 \\ 10^{-11.41}(\gamma_{H^+}[H^+])^{0.18}\left[\frac{mol}{cm^2 \cdot s}\right], & pH > 4.8 \end{cases} \quad (13)$$

where a_v is the available surface area for reaction per unit volume of the cement slurry. Monocalcium silicate particles of the NYAD M400 used in this study have a specific surface area of 2.0 m^2/g as measured by a BET surface area analyzer (Tristar II 3020, Micromeritics, Inc., GA, USA). For a 15 wt % cement slurry, $a_v = 3.33 \times 10^6$ cm^2/L. It is assumed that all the reaction rates reduce to 0 when conditions are no longer favorable for the reaction to proceed. For example, once all the urea is consumed, $r_{urease} = 0$. Similarly, if calcium and carbonate ion concentrations are not high enough to initiate precipitation, i.e., $[Ca^{2+}][CO_3^{2-}] < K_6$, then $r_{calcite} = 0$.

To investigate the use of acetic acid incubation to facilitate ICD prior to microbe/urea addition, extra equations describing the acid equilibrium and the mass balance of the acid are included. The acid equilibrium equation is given by the following:

$$CH_3COOH \rightarrow H^+ + CH_3COO^- \quad (14)$$

The mass balance on the amount of the acid added yields the following:

$$[CH_3COOH]_t + [CH_3COO^-]_t = acid_{tot} \quad (15)$$

It is assumed that the anion CH_3COO^- does not participate in any other reaction and does not precipitate as any solid. Table S2 tabulates the equilibrium constant for acetic acid.

Thermal Modeling of Carbonation of Monocalcium Silicate. The overall carbonation of monocalcium silicate is known to be an exothermic reaction[36] and is thus expected to increase the temperature of the system. To estimate the expected temperature range during the carbonation of monocalcium silicate, an energy balance was performed by assuming adiabatic conditions and constant heat capacities. The assumption of adiabatic conditions implies that there is no heat loss to the environment and all the heat generated due to the reaction is used to increase the temperature of the unreacted reactants, generated products, and inert compounds (e.g., water). This assumption will yield an upper limit to the expected temperature increase. Note that any heat consumed in dissolving the urea in water is not considered. The exothermic reaction considered in this model is as follows:

$$CaSiO_3 + CO_2 \rightarrow CaCO_3 + SiO_2 \quad (16)$$

The adiabatic energy balance results in the following equation:

https://doi.org/10.1021/acsomega.1c05264
ACS Omega 2022, 7, 12524−12535

$$\frac{\phi V\rho_{H_2O}}{M_{H_2O}}C_{p,H_2O}(T_f - T_0) + (1-\xi)\frac{(1-\phi)V\rho_W}{M_W}C_{p,W}(T_f - T_0) + \xi\frac{(1-\phi)V\rho_W}{M_W}C_{p,S}(T_f - T_0) + \xi\frac{(1-\phi)V\rho_W}{M_W}C_{p,C}(T_f - T_0) + \Delta H\xi\frac{(1-\phi)V\rho_W}{M_W} = 0 \Rightarrow T_f = T_0 - \Delta H\xi\frac{(1-\phi)\rho_W}{M_W}\left[\frac{\phi\rho_{H_2O}}{M_{H_2O}}C_{p,H_2O} + (1-\xi)\frac{(1-\phi)\rho_W}{M_W}C_{p,W} + \xi\frac{(1-\phi)\rho_W}{M_W}(C_{p,S} + C_{p,C})\right]^{-1} \quad (17)$$

where ϕ is the porosity of the initial slurry; V is the volume of the system; ρ_i, M_i, and $C_{p,i}$ are the density, molecular weight, and specific heat capacity of component i, respectively; T_f is the final temperature of the system; T_0 is the initial temperature of the system; ξ is the extent of reaction; and ΔH is the enthalpy of reaction. Subscripts H_2O, W, S,and C indicate water, monocalcium silicate, silica, and calcium carbonate, respectively. The porosity of the initial slurry, ϕ, is related to the weight fraction of monocalcium silicate, w, by the following equation:

$$\phi = \frac{\frac{w}{\rho_W}}{\frac{w}{\rho_W} + \frac{1-w}{\rho_{H_2O}}} \quad (18)$$

Since the analysis does not include the enthalpy of water vaporization, the model is invalid at temperatures higher than 100 °C. The parameter values of the constants used in eq 17 are listed in Table S3.

Carbonate Content Determination. The carbonate content of all monocalcium silicate samples was assessed using a calcimeter according to the manufacturer's recommendations (Eijkelkamp Soil & Water, The Netherlands). Deionized water was utilized as a solvent. Hydrochloric acid (4 mol L^{-1}) was diluted from PlasmaPure 34−37% (concentrated) hydrochloric acid (SCP Science, Canada). ACS reagent-grade (≥99.0%) calcium carbonate (Millipore-Sigma, USA) was used for column calibration. All samples prior to calcimetry were harvested via vacuum filtration through Grade 151 Ahlstrom glass microfiber filters (VWR International, USA), washed with deionized water to remove all soluble phases, and dried at 70 °C and a 20 in. Hg vacuum pressure using a VWR 1430M vacuum oven. Sample sizes were adjusted between 1.0 and 3.0 g such that the generated carbon dioxide pressure fell within the linear calibration range (20−80 mL). The carbonate content (g per kg) of the total powder mass was calculated according to the manufacturer's recommendation (Eijkelkamp Soil & Water, The Netherlands). The carbonate content (molar percent conversion of the original monocalcium silicate) was calculated as an extension of the original carbonate content (g carbonate per kg total powder) with the following assumptions: (1) the only phases present are $CaCO_3$, SiO_2, and $CaSiO_3$, and (2) $CaCO_3$ and SiO_2 are present in equimolar amounts (i.e., 1:1). The mol % conversion is defined relative to the starting molar quantity of $CaSiO_3$ according to the following equations:

$$CaSiO_3(s) + 2CH_3COOH(aq) \rightleftarrows Ca(CH_3COO)_2(aq) + SiO_2(s) + H_2O(l) \quad (19)$$

$$Ca(CH_3COO)_2(aq) + (NH_2)_2CO(aq) + 2H_2O(l) \rightleftarrows CaCO_3(s) + 2NH_4CH_3COO(aq) \quad (20)$$

Evolution of the Carbonate Phase with Respect to the Acid Content. Powder X-ray diffraction (XRD) was used to assess the crystalline phase composition of all samples. XRD was conducted using a Bruker D8 Discover (Bruker AXS, USA) with a step size of 0.018° (2θ) with a 0.5 s dwell time. The instrument was equipped with a Vantec 1 detector, a Cu Kα source operating at 40 kV and 40 mA (1600 W), and a horizontal goniometer. Pattern analysis was conducted using MDI Jade (Materials Data, Inc., USA) equipped with the International Centre for Diffraction Data 711 database (ICDD, USA) to determine the identity of the constituent phases. All samples prior to XRD analysis were processed as described in the "Carbonate Content Determination" section.

Scanning Electron Microscopy and Elemental Analysis. After 72 h of incubation, the monocalcium silicate slurries were centrifuged (5000g for 10 min), rinsed with deionized water, dried, gold-coated by a sputter, and scanned by SEM at 300×, 1000×, 5000×, and 10,000× magnifications at 5 kV (Thermo Scientific Apreo 2 SEM, USA). Energy-dispersive X-ray (EDX) analysis was conducted at 15 kV for elemental analysis.

■ ASSOCIATED CONTENT

Supporting Information

The Supporting Information is available free of charge at https://pubs.acs.org/doi/10.1021/acsomega.1c05264.

Screening and selection of ureolytic microbes; modeled microbial calcium carbonate precipitation rates; thermal urea decomposition rates; values for thermal equilibrium constants; parameter values for thermal models (PDF)

■ AUTHOR INFORMATION

Corresponding Authors

Richard E. Riman − *Department of Materials Science & Engineering, Rutgers—The State University of New Jersey, Piscataway, New Jersey 08854, United States;* orcid.org/0000-0002-4289-5768; Email: riman@rutgers.edu

Yongqin Jiao − *Physical and Life Sciences Directorate, Lawrence Livermore National Laboratory, Livermore, California 94550, United States;* orcid.org/0000-0002-6798-5823; Email: jiao1@llnl.gov

Authors

Michael S. Guzman − *Physical and Life Sciences Directorate, Lawrence Livermore National Laboratory, Livermore, California 94550, United States;* orcid.org/0000-0002-3888-8055

Jaisree Iyer − *Physical and Life Sciences Directorate, Lawrence Livermore National Laboratory, Livermore, California 94550, United States;* orcid.org/0000-0002-1154-3030

Paul Kim − *Department of Materials Science & Engineering, Rutgers—The State University of New Jersey, Piscataway, New Jersey 08854, United States;* orcid.org/0000-0002-1544-2309

Daniel Kopp − *Department of Materials Science & Engineering, Rutgers—The State University of New Jersey, Piscataway, New Jersey 08854, United States*

https://doi.org/10.1021/acsomega.1c05264
ACS Omega 2022, 7, 12524−12535

Ziye Dong − *Physical and Life Sciences Directorate, Lawrence Livermore National Laboratory, Livermore, California 94550, United States;* orcid.org/0000-0002-0419-8523
Paniz Foroughi − *Department of Materials Science & Engineering, Rutgers—The State University of New Jersey, Piscataway, New Jersey 08854, United States*
Mimi C. Yung − *Physical and Life Sciences Directorate, Lawrence Livermore National Laboratory, Livermore, California 94550, United States*

Complete contact information is available at: https://pubs.acs.org/10.1021/acsomega.1c05264

Notes

The authors declare no competing financial interest.

■ ACKNOWLEDGMENTS

The Advanced Research Project Agency-Energy (ARPA-E) within the Department of Energy (DOE) supported this work. The authors would like to thank Imerys Performance Additives for providing the monocalcium silicate utilized in this work, Dr. Megan Smith for her advice on the geochemical modeling, and Dr. Larry Dugan for providing the *Bacillus megaterium* strain used in this study. This work was performed under the auspices of the U.S. Department of Energy by the Lawrence Livermore National Laboratory under Contract DE-AC52-07NA27344 (LLNL-JRNL-821769).

■ REFERENCES

(1) Worrell, E.; Price, L.; Martin, N.; Hendriks, C.; Meida, L. O. Carbon dioxide emissions from the global cement industry. *Annu. Rev. Energy* **2001**, *26*, 303−329.
(2) *Tracking Industrial Energy Efficiency and CO_2 Emissions*. IEA, June 2007. https://www.iea.org/reports/tracking-industrial-energy-efficiency-and-co2-emissions (accessed 2021-09-22).
(3) Huang, H.; Wang, T.; Kolosz, B.; Andresen, J.; Garcia, S.; Fang, M.; Maroto-Valer, M. M. Life-cycle assessment of emerging CO_2 mineral carbonation-cured concrete blocks: Comparative analysis of CO_2 reduction potential and optimization of environmental impacts. *J. Cleaner Prod.* **2019**, *241*, No. 118359.
(4) Riman, R. E.; Gupta, S.; Atakan, V.; Li, Q. Bonding element, bonding matrix and composite material having the bonding element, and method of manufacturing thereof. US 9,868,667, 2018.
(5) Riman, R. E.; Atakan, V.; Kuppler, J. P.; Smith, K. M. Precursors and transport methods for hydrothermal liquid phase sintering (HLPS). US 9,266,147, 2016.
(6) Li, Q.; Gupta, S.; Tang, L.; Quinn, S.; Atakan, V.; Riman, R. E. A novel strategy for carbon capture and sequestration by rHLPD processing. *Front. Energy Res.* **2016**, *3*, 53.
(7) Riman, R. E.; Atakan, V. Systems and methods for carbon capture and sequestration and compositions derived therefrom. US 8,114,367, 2012.
(8) Riman, R. E.; Atakan, V. Method of hydrothermal liquid phase sintering of ceramic materials and products derived therefrom. US 8,313,802, 2010.
(9) Stocks-Fischer, S.; Galinat, J. K.; Bang, S. S. Microbiological precipitation of $CaCO_3$. *Soil Biol. Biochem.* **1999**, *31*, 1563−1571.
(10) Røyne, A.; Phua, Y. J.; Balzer Le, S.; Eikjeland, I. G.; Josefsen, K. D.; Markussen, S.; Myhr, A.; Throne-Holst, H.; Sikorski, P.; Wentzel, A. Towards a low CO_2 emission building material employing bacterial metabolism (1/2): The bacterial system and prototype production. *PLoS One* **2019**, *14*, No. e0212990.
(11) Choi, S. G.; Chu, J.; Brown, R. C.; Wang, K.; Wen, Z. Sustainable biocement production via microbially induced calcium carbonate precipitation: Use of limestone and acetic acid derived from pyrolysis of lignocellulosic biomass. *ACS Sustainable Chem. Eng.* **2017**, *5*, 5183−5190.
(12) Di Lorenzo, F.; Ruiz-Agudo, C.; Ibañez-Velasco, A.; Millán, R. G.-S.; Navarro, J. A. R.; Ruiz-Agudo, E.; Rodriguez-Navarro, C. The carbonation of wollastonite: A model reaction to test natural and biomimetic catalysts for enhanced CO_2 sequestration. *Minerals* **2018**, *8*, 209.
(13) Zhao, H.; Park, Y.; Lee, D. H.; Park, A.-H. A. Tuning the dissolution kinetics of wollastonite via chelating agents for CO_2 sequestration with integrated synthesis of precipitated calcium carbonates. *Phys. Chem. Chem. Phys.* **2013**, *15*, 15185−15192.
(14) Daval, D.; Martinez, I.; Corvisier, J.; Findling, N.; Goffé, B.; Guyot, F. Carbonation of Ca-bearing silicates, the case of wollastonite: Experimental investigations and kinetic modeling. *Chem. Geol.* **2009**, *265*, 63−78.
(15) Lauchnor, E. G.; Topp, D. M.; Parker, A. E.; Gerlach, R. Whole cell kinetics of ureolysis by *Sporosarcina pasteurii*. *J. Appl. Microbiol.* **2015**, *118*, 1321−1332.
(16) Kim, G.; Kim, J.; Youn, H. Effect of Temperature, pH, and Reaction Duration on Microbially Induced Calcite Precipitation. *Appl. Sci.* **2018**, *8*, 1277.
(17) Whiffin, V. S. Microbial $CaCO_3$ precipitation for the production of biocement. Ph.D. Dissertation, Murdoch University, Perth, Australia, 2004.
(18) Phua, Y. J.; Røyne, A. Bio-cementation through controlled dissolution and recrystallization of calcium carbonate. *Constr. Build. Mater.* **2018**, *167*, 657−668.
(19) Myhr, A.; Røyne, F.; Brandtsegg, A. S.; Bjerkseter, C.; Throne-Holst, H.; Borch, A.; Wentzel, A.; Røyne, A. Towards a low CO_2 emission building material employing bacterial metabolism (2/2): Prospects for global warming potential reduction in the concrete industry. *PLoS One* **2019**, *14*, No. e0208643.
(20) Sauer, M.; Porro, D.; Mattanovich, D.; Branduardi, P. Microbial production of organic acids: Expanding the markets. *Trends Biotechnol.* **2008**, *26*, 100−108.
(21) Cuthbert, M. O.; Riley, M. S.; Handley-Sidhu, S.; Renshaw, J. C.; Tobler, D. J.; Phoenix, V. R.; Mackay, R. Controls on the rate of ureolysis and the morphology of carbonate precipitated by *S. pasteurii* biofilms and limits due to bacterial encapsulation. *Ecol. Eng.* **2012**, *41*, 32−40.
(22) Mitchell, A. C.; Espinosa-Ortiz, E. J.; Parks, S. L.; Phillips, A. J.; Cunningham, A. B.; Gerlach, R. Kinetics of calcite precipitation by ureolytic bacteria under aerobic and anaerobic conditions. *Biogeosciences* **2019**, *16*, 2147−2161.
(23) Ma, L.; Pang, A. P.; Luo, Y. S.; Lu, X. L.; Lin, F. M. Beneficial factors for biomineralization by ureolytic bacterium *Sporosarcina pasteurii*. *Microb. Cell. Fact.* **2020**, *19*, 1−12.
(24) Castro-Alonso, M. J.; Montañez-Hernandez, L. E.; Sanchez-Muñoz, M. A.; Macias Franco, M. R.; Narayanasamy, R.; Balagurusamy, N. Microbially Induced Calcium carbonate Precipitation (MICP) and its potential in bioconcrete: Microbiological and molecular concepts. *Front. Mater.* **2019**, *6*, 126.
(25) Martinez, B.; Barkouki, T.; DeJong, J.; Ginn, T. Upscaling microbial induced calcite precipitation in 0.5 m columns: Experimental and modeling results. *Geo-Frontiers 2011: Advances in Geotechnical Engineering*; American Society of Civil Engineers, 2011; pp 4049−4059.
(26) Almajed, A.; Tirkolaei, H. K.; Kavazanjian, E., Jr.; Hamdan, N. Enzyme induced biocementated sand with high strength at low carbonate content. *Sci. Rep.* **2019**, *9*, 1135.
(27) Nemati, M.; Greene, E. A.; Voordouw, G. Permeability profile modification using bacterially formed calcium carbonate: comparison with enzymic option. *Process Biochem.* **2005**, *40*, 925−933.
(28) Bang, S. S.; Galinat, J. K.; Ramakrishnan, V. Calcite precipitation induced by polyurethane-immobilized *Bacillus pasteurii*. *Enzyme Microb. Technol.* **2001**, *28*, 404−409.
(29) Zhang, W.; Ju, Y.; Zong, Y.; Qi, H.; Zhao, K. In situ real-time study on dynamics of microbially induced calcium carbonate precipitation at a single-cell level. *Environ. Sci. Technol.* **2018**, *52*, 9266−9276.

(30) Ghosh, T.; Bhaduri, S.; Montemagno, C.; Kumar, A. *Sporosarcina pasteurii* can form nanoscale calcium carbonate crystals on cell surface. *PLoS One* **2019**, *14*, No. e0210339.
(31) Cordero, I.; Snell, H.; Bardgett, R. D. High throughput method for measuring urease activity in soil. *Soil Biol. Biochem.* **2019**, *134*, 72−77.
(32) Bethke, C. M. *Geochemical and Biogeochemical Reaction Modeling*; Cambridge University Press: New York, 2007.
(33) Helgeson, H. C. Thermodynamics of hydrothermal systems at elevated temperatures and pressures. *Am. J. Sci.* **1969**, *267*, 729−804.
(34) Wolery, T. J. *EQ3/6 A Software Package for Geochemical Modeling*; Lawrence Livermore National Laboratory: Livermore, CA 2010.
(35) Schott, J.; Pokrovsky, O. S.; Spalla, O.; Devreux, F.; Gloter, A.; Mielczarski, J. A. Formation, growth and transformation of leached layers during silicate minerals dissolution: The example of wollastonite. *Geochim. Cosmochim. Acta* **2012**, *98*, 259−281.
(36) Lackner, K. S.; Wendt, C. H.; Butt, D. P.; Joyce, E. L., Jr.; Sharp, D. H. Carbon dioxide disposal in carbonate minerals. *Energy* **1995**, *20*, 1153−1170.

https://doi.org/10.1021/acsomega.1c05264
ACS Omega 2022, 7, 12524−12535